Thermodynamics of tubelike flexible polymers

Thomas Vogel,[1] Thomas Neuhaus,[2] Michael Bachmann,[1,3] and Wolfhard Janke[1]

[1]*Institut für Theoretische Physik and Centre for Theoretical Sciences (NTZ), Universität Leipzig, Postfach 100 920, 04009 Leipzig, Germany*

[2]*Jülich Supercomputing Centre, Forschungszentrum Jülich, 52425 Jülich, Germany*

[3]*Institut für Festkörperforschung, Theorie II, Forschungszentrum Jülich, 52425 Jülich, Germany*

In this work, we discuss the general phase behavior of short tubelike flexible polymers. The geometric thickness constraint is implemented through the concept of the global radius of curvature. We use sophisticated Monte Carlo sampling methods to simulate small bead-stick polymer models with Lennard-Jones interaction among nonbonded monomers. We analyze energetic fluctuations and structural quantities to classify conformational pseudophases. We find that the tube thickness influences the thermodynamic behavior of simple tubelike polymers significantly, i.e., for a given temperature, the formation of secondary structures strongly depends on the tube thickness.

I. INTRODUCTION

To resolve the conformational mechanics of secondary-structure formation is one of the major tasks in polymer science. While in the "real world" experiments are restricted to specific molecules under specific conditions, in the "virtual world" of computer simulations there are no such limitations. Using reasonably simplified models, systematic studies of classes of polymers in different environments are possible [1].

A common, effective, and widely used coarse-grained model for polymers is the bead-stick model [2,3]. Here, the polymer is modeled as a linear chain of pointlike monomers, which correspond to molecular units, e.g., amino acid residues in the case of proteins. The monomers are connected by stiff bonds and interact via simple effective pair potentials. This class of models enables computer simulations of very large polymer systems and is, for example, quite useful for studying the global structure formation or structural transitions [4–6]. On the other hand, due to the simple pairwise interactions, it is hardly possible to investigate the formation of secondary structures in a systematic way, which is due to missing specific extensions such as hydrogen bonds, anisotropy, explicit stiffness, etc. [7–10].

In this work, we therefore follow the approach introduced by Banavar, Maritan, and co-workers [11–13], where a tubelike model is considered instead of linelike chains. The virtual thickness of the tube caused by the bulky shape of the monomers (e.g., because of side chains connected to the backbone) is introduced via a three-body interaction. The general tertiary phase behavior of tubelike polymers with 40 and more monomers has already been investigated using a square-well model [11], identifying the folding and collapse transitions in a structural phase diagram parametrized by thickness and temperature. In our study, we investigate in detail the thickness and temperature dependence of the secondary-structure formation of tube polymers, employing a continuum model with intermonomeric Lennard-Jones potential. For this reason, we consciously investigate rather small chains (with up to 13 monomers). For longer chains, tertiary folding effects become apparently important and symmetry, anisotropy, and marginal compactness of globular protein structures are then doubtlessly of interest [14,15]. However, the globular arrangement of secondary segments in tertiary folds is not in the focus of this study and it is also hardly feasible to perform a similarly precise analysis of the present work for longer chains.

The present work extends our recent study of ground-state properties of tubelike polymers as a function of their thickness [16,17]. Thus, the conformations found in these former studies represent the dominant structures in the fluctuation free, i.e., lowest-temperature region $(T \to 0)$ of the entire conformational phase diagram that we will discuss in detail in the following. Thus, the goal of this study is to identify independently of the chain length the relevant pseudophases in the thermodynamic phase diagram based on the shape of ground-state structures. The notion "phase" shall be handled with some care; conformational phase transitions of small systems are not thermodynamic phase transitions in a strict sense. Nonetheless, there is a strong similarity of these structural transitions and thermodynamic phase transitions, as both are typically governed by the competition of energy and entropy. However, to make clear that there can also be significant differences (no collapse of fluctuating quantities, i.e., there are transition regions rather than transition points), we call conformational phases of short chains "pseudophases" in the following [18].

Recent related studies also apply other tube models for homopolymers to investigate the formation of secondary-structures (see, e.g., Refs. [19–23]). These are, however, based on different approaches to influence or potentiate the structure formation (see, e.g., the discussion in Ref. [16]).

The rest of the paper is organized as follows. In Sec. II, we describe the model and specify the simulation methods we employed. In Sec. III, we present the complete thermodynamic phase diagrams for various chain lengths of homopolymers and analyze and classify the different pseudophases therein. In Sec. IV, we introduce a hydrophobic-polar heteropolymer tube model and analyze the ensuing pseudophase behavior for an exemplified se-
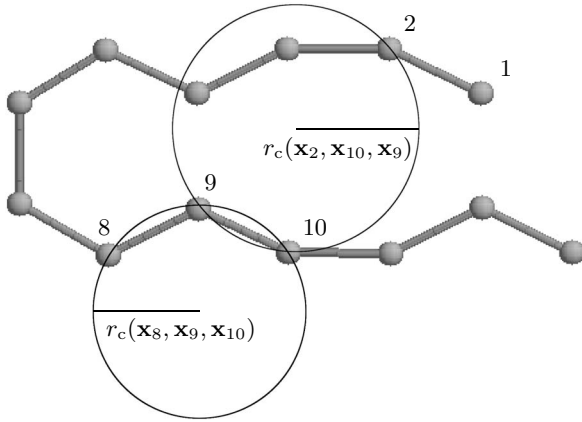
FIG. 1. Two examples of circumcircles of three monomers and the corresponding radii of curvature. The small circle corresponds to the radius of curvature of three consecutive monomers, i.e., to the local radius of curvature of the monomers $(i, i+1, i+2) = (8, 9, 10)$. The bigger circle corresponds to the radius of curvature r_c of the monomers $(i, j, k) = (2, 10, 9)$.

quence of monomers. Finally, our main findings are summarized in Sec. V.

II. MODEL AND METHODS

As outlined above, we employ in this study a linear flexible polymer model with thickness, i.e., we consider tubelike chains instead of linelike objects. The bond length in this model is kept fixed, i.e., $r_{i,i+1} = 1$, where $r_{i,j} = |\mathbf{x}_i - \mathbf{x}_j|$ denotes the distance between two monomers. The monomers interact via a standard Lennard-Jones (12,6)-potential resulting from pairwise attractive van der Waals and short-range repulsion forces,

$$V_{\mathrm{LJ}}(r_{i,j}) = 4\epsilon \left[\left(\frac{\sigma}{r_{i,j}} \right)^{12} - \left(\frac{\sigma}{r_{i,j}} \right)^{6} \right]. \qquad (1)$$

In the following, we set $\sigma = \epsilon = 1$, such that V_{LJ} vanishes for $r_{i,j} = 1$ and is minimal at $r_{i,j}^{\min} = 2^{1/6} \approx 1.122$ with $V_{\mathrm{LJ}}(r_{i,j}^{\min}) = -1$. The total energy of a conformation $\mathbf{X} = (\mathbf{x}_1, \ldots, \mathbf{x}_N)$ is then calculated as the sum of all LJ contributions, $E(\mathbf{X}) = \Sigma_{i,j>i+1} V_{\mathrm{LJ}}(r_{i,j})$.

To define the thickness of a conformation $\mathbf{X}$, we apply the concept of the global radius of curvature [24]. Accordingly, we measure all (see technical remark below) radii of curvature $r_c(\mathbf{x}_i, \mathbf{x}_j, \mathbf{x}_k)$, i.e., the radii of the circles defined by the monomer positions $\mathbf{x}_i$, $\mathbf{x}_j$, and $\mathbf{x}_k$. The minimal radius of curvature is called the global radius of curvature,

$$r_{\mathrm{gc}}(\mathbf{X}) := \min\{r_c(\mathbf{x}_i, \mathbf{x}_j, \mathbf{x}_k) | \ \forall \ i, j, k; i \neq j \neq k\}. \qquad (2)$$

The thickness $d(\mathbf{X})$ of the polymer tube is simply twice the global radius of curvature $d(\mathbf{X}) = 2r_{\mathrm{gc}}(\mathbf{X})$. For illustration, Fig. 1 shows two radii of curvature of a conformation with $N = 13$ monomers. As a technical remark: the explicit calculation of all radii of curvature is obviously needless and would be very expensive in terms of computing time as the number of radii grows with the third power of the monomer number [$\mathcal{O}(N^3)$]. By excluding a huge number of *a priori* too

large radii with much less effort, the calculation can be done nearly in $\mathcal{O}(N \log N)$ steps (possibly plus some marginal higher-order terms) [25]. In order to simulate the model, we restrict the conformational space by a thickness constraint ρ, such that conformations with $r_{\mathrm{gc}} < \rho$ are forbidden, i.e., the Heaviside function $\Theta(r_{\mathrm{gc}}(\mathbf{X}) - \rho)$ is included in the partition function,

$$Z = \int \mathcal{D}X \Theta(r_{\mathrm{gc}}(\mathbf{X}) - \rho) e^{-\beta E(\mathbf{X})}, \qquad (3)$$

where $\mathcal{D}X$ is the functional-integral measure and $\beta = 1/k_B T$ is the inverse temperature (with $k_B = 1$ in natural units). For a more detailed description and discussion of the concept and its applicability to polymer models, see, for example, Refs. [12,13,16,17].

In our Monte Carlo simulations, we use multicanonical flat-histogram sampling [26,27] to estimate the density of states. To determine the weight factors, we employ the recursive method of Wang and Landau [28], with the control parameter f initialized and subsequently decreased to $f - 1 < 10^{-7}$, as described in Ref. [29]. We remark that for any finite value $f - 1$, the Markov chain of configurations, as generated with the Wang-Landau algorithm, does not possess a proper Gibbs measure. Rather, the density of states, entering here the Metropolis criterion, is constantly updated and hence varies as the Markov chain proceeds. Thus, the detailed balance is violated, in particular, in the initial simulation phase. We therefore decided to freeze the weights at some point of the Wang-Landau iteration and to perform a multicanonical production run with a Gibbs measure as determined by the multicanonical weight factor. Furthermore, we also checked our results for reliability against data obtained by parallel tempering simulations [25,30–32], which generate simultaneous ensembles of polymers at a multitude of temperature values. The checks are done for selected parameter sets, as well as against data from the study presented in Ref. [33]. The simulations of different polymer lengths and thickness constraint values were carried out separately to avoid correlations and statistical imbalances.

III. CONFORMATIONAL PHASE DIAGRAMS OF TUBELIKE HOMOPOLYMERS

A. General

In this work, we study homopolymers consisting of $N = 8$, 9, 10, and 13 monomers. After having considered the low-temperature regime, i.e., ground states, elsewhere [17], we here concentrate on the conformational phase behavior at finite temperatures. As common, we calculate the specific heat and consider the peak regions of this observable as indicators of relevant thermodynamical activity. Figure 2 shows these specific-heat landscapes for the $N = 8$ and $N = 9$ polymers. The points (+) plotted in the top-view representation of Fig. 2(c) and Fig. 2(d) indicate the positions of the crest lines in this landscape, i.e., the lines signaling structural changes. We notice four major pseudophases, which we denote by α, β, γ, and δ. In Fig. 3, we show the corresponding canonical energy histograms at temperature $T = 0.1$ for differ-
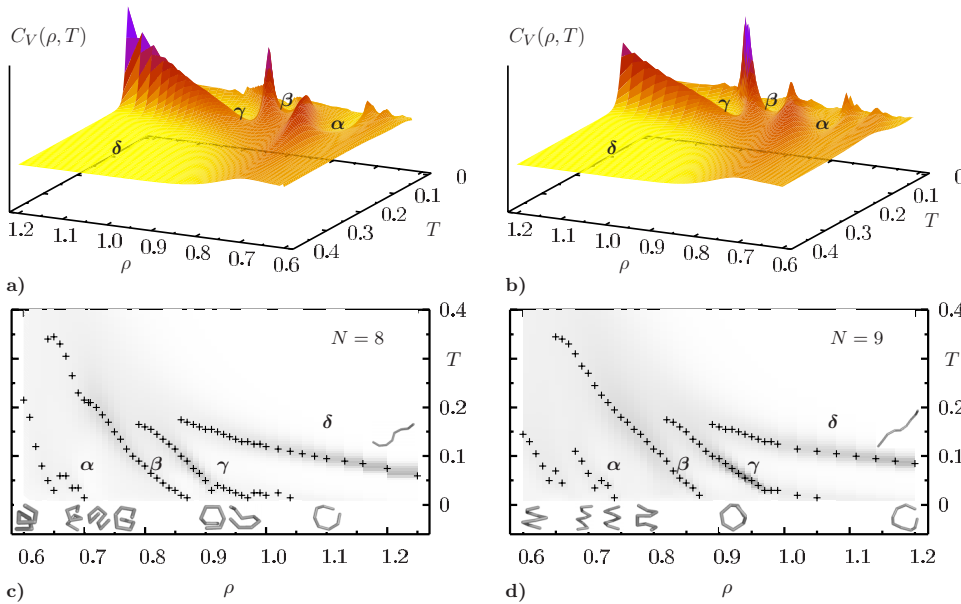
FIG. 2. (Color online) Phase diagrams of the homopolymers with $N=8$ (left) and $N=9$ (right). The labels α, β, γ, and δ indicate the different pseudophases at finite temperature. (a) and (b) show the perspective view of the specific-heat landscape and, in (c) and (d), the top views are plotted with marked peak positions for various parameters ρ. The specific-heat values are encoded in grayscale. The pictures in the insets in (c) and (d) correspond to the ground states presented in Ref. [17]; the pictures in the δ regions show relevant conformations there.

ent thickness constraints ρ, with the histograms at the transition values of ρ marked by arrows. Both plots, for $N=8$ and $N=9$, do not differ qualitatively, i.e., have all interesting features in common. The phase structure will be discussed in the subsequent detailed analysis of the pseudophase diagrams.

In the insets of Figs. 2(c) and 2(d), ground-state conformations, according to their thickness, are shown. They provide a first indication for the population of the respective pseudophase at finite temperatures. Deeper analyses will strengthen the expectation that the ground-state conformations are the relevant conformations in the corresponding pseudophases at finite temperatures as well. This includes, for example, the analyses of distributions of structural observables such as end-to-end distance, radius of gyration, radial distribution of monomers, bond and torsion angles, as well as comparisons with reference structures and "counting" structural components, e.g., using pattern recognition [34], during additional canonical simulations at fixed temperatures. Let us note that we neglect data for $\rho \lesssim 0.6$, which

corresponds to the pure Lennard-Jones volume exclusion, as the thickness constraint does not influence the system at all below this "natural thickness" [17].

B. Analysis of structural phases

We begin the detailed discussion of the different structural phases with the high-thickness region, i.e., with the phase γ and the transition to δ. Based on the knowledge of the ground states and some general structural properties of polymers, we assume in γ a population of bended rings, which undergo a structural change to sprawled random coils in δ, which become more and more rodlike with increasing thickness. This assumption can be illustrated and strengthened by an example in little more detail. For $N=8$ monomers, let us consider the geometrical objects "octagon" and "straight line" as limiting prototypes of these regions. Calculating the properties of these prototypes, one expects for the end-to-end distance distributions a sharp peak at the position of the LJ potential minimum, i.e., at $r_{\text{end}} \approx 1.12$, and a diffuse peak at
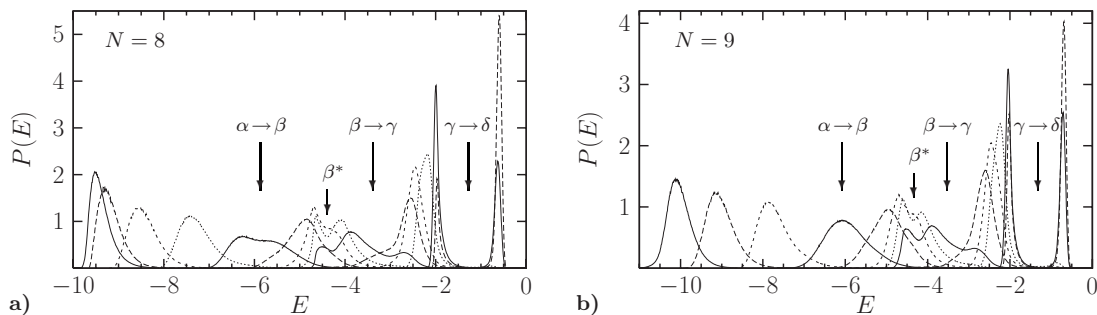

FIG. 3. Energy histograms for various thickness constraints ρ at $T=0.1$. Histograms corresponding to specific-heat maxima are marked with arrows. (a) $N=8$ polymer. Histograms correspond to the following thickness parameters: $\rho=0.7$ (solid line), 0.72, 0.74, 0.76, 0.78 (solid line, $\alpha \rightarrow \beta$), 0.8, 0.82, 0.84, 0.86 (solid line, $\beta \rightarrow \gamma$), 0.88, 0.9, 0.95, 1.08 (solid line, $\gamma \rightarrow \delta$), 1.13. (b) $N=9$ polymer. Histograms correspond to $\rho=0.72$ (solid line), 0.75, 0.78, 0.81 (solid line, $\alpha \rightarrow \beta$), 0.83, 0.85, 0.87, 0.89 (solid line, $\beta \rightarrow \gamma$), 0.92, 0.95, 1.11 (solid line, $\gamma \rightarrow \delta$), 1.14. The histograms were obtained by reweighting the density of states and are consistent with histograms obtained from independent canonical simulations at this temperature. These histograms contain about 10^{10} entries. Statistical errors are less than 1% and, almost everywhere, smaller than the linewidth.
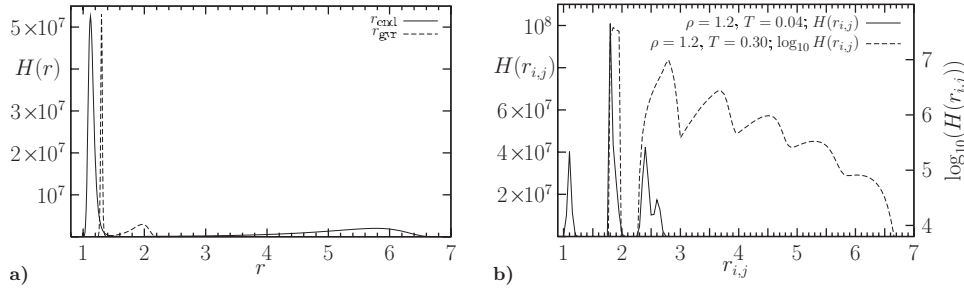
FIG. 4. Measured histograms from simulations at fixed temperatures for the $N=8$ polymer (a) at the transition from the bended-ring phase γ to the sprawled-coil phase δ and (b) deep inside these two phases. (a) End-to-end distance (solid line) and radius of gyration (dashed line) at the $\gamma \leftrightarrow \delta$ transition ($\rho=1.08$ and $T=0.1$). (b) Radial distribution ($\rho=1.2$) in the bended-ring phase γ (solid line, $T=0.04$) and in the sprawled-coil phase δ (dashed line, $T=0.3$). The histograms are differently scaled for better visibility, each contains more than 10^9 entries. Statistical errors are less than 1% and smaller than the linewidth.

$r<7$, for the radius of gyration distribution a sharp peak at $r_{\text{gyr}} \approx 1.3$ and a diffuse peak at $r<2.34$, and for the radial distribution function sharp peaks at $r \approx 1.1$, 1.8, 2.35, and 2.55 and smooth peaks close to integer values for the respective conformations. In Fig. 4, these distributions, as measured in canonical simulations at the transition temperature and within the two phases, are shown. In Fig. 4(a), the end-to-end distance and radius of gyration histograms are plotted, and Fig. 4(b) shows the radial distribution function. These quantities exhibit exactly the assumed behavior, i.e., the peaks of the measured distributions appear exactly at the calculated values for the anticipated "prototypes." Additionally, the bimodal shapes of the distributions in Fig. 3 at the transition $\gamma \rightarrow \delta$ are an indication for the first-order-like character of this transition with coexisting conformational phases. The energy histograms near the transition point exhibit two distinct peaks separated by broad energy gaps. During simulations at the transition line, both structures appear equally, as can be seen, for example, in Fig. 4(a).

Reducing the thickness parameter ρ, we reach the phase β, which we call the sheet phase. Figure 5 shows the results of simulations at $\rho=0.82$ and $T=0.1$ for the $N=8$ polymer, which belongs to the region called β^* in Fig. 3(a). There are mainly three structures dominating the phase β, among them the two ground-state conformations in the range $0.89 \leq \rho \leq 0.99$ (cp. Ref. [17] and Fig. 2). As shown in Fig. 5(a), they can be distinguished with the help of the end-to-end distance, where three distinct peaks in the distribution appear, whereas they cannot be resolved in terms of the specific heat. The plot in Fig. 5(b) shows the overall energy distribution as well as the contributions from the three regions corresponding to the peaks in the end-to-end distribution. As illustrated in Fig. 5(d), the peak in the energy distribution is associated with ringlike conformations and their excitations, whereas the
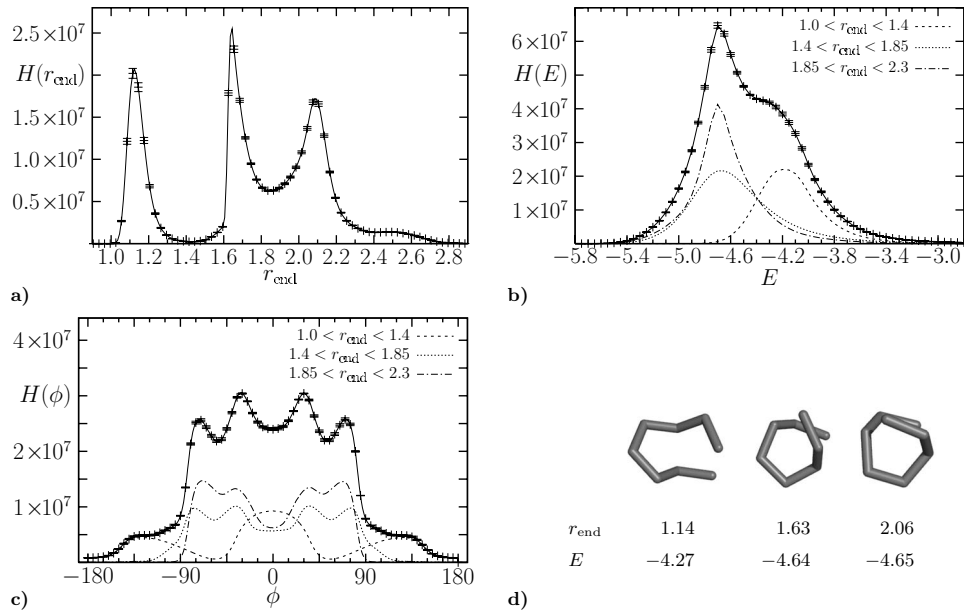

FIG. 5. Measured histograms in phase β for $\rho=0.82$ and $T=0.1$ for the $N=8$ polymer. (a) The end-to-end distance histogram exhibits three separate peaks indicating three different major contributing groups of conformations. (b) The energy histogram and (c) the histogram of torsional angles. Error bars were obtained from independent simulations and are shown exemplarily. In (b) and (c), the histograms for each group of conformations distinguished by its end-to-end distance are shown in addition. Each histogram contains at least 10^9 entries. (d) Representatives of each group of this energetic pseudophase and their corresponding properties.
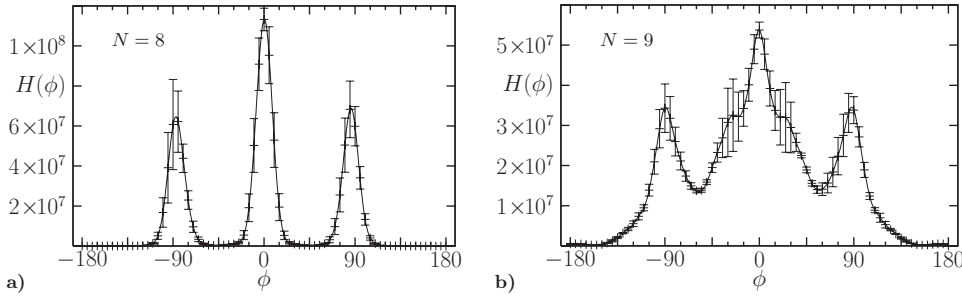
FIG. 6. Torsion angle distributions at $T=0.1$ for the (a) $N=8$ and (b) $N=9$ polymers in phase α at $\rho=0.7$ and $\rho=0.72$, respectively (cuboid or sc-helical region). Each histogram contains about 10^{10} entries. For visualizations of corresponding conformations, see, e.g., Fig. 2(c).

shoulder is caused by hairpinlike conformations. In Fig. 5(c), we plot the distribution of torsion angles. The contributions of the different structural classes can be distinguished very well again. One notes, for example, an accumulation of torsion angles around $\phi=0$ in the contribution of the hairpinlike conformations: an indication for the planar structure of the conformation. At β^{*}, the conformations extend into the third dimension, i.e., bonds within the conformations begin to overlap. An analogous behavior is found for $N=9$ [see Fig. 3(b)].

The region of lowest thickness α is the helical phase. This phase can be further separated into subphases, where in one of them the exact α helix resides as a ground state for $N=8$ and $N=9$ [17]. In a further region, simple-cubic helical structures [35] or cuboids for $N=8$, corresponding to the ground-state conformations in the range $1/\sqrt{2}\approx0.707\lesssim\rho\lesssim0.8$, respectively, dominate [36]. These regions are separated by noticeable—but in the context of the whole phase diagram less important—transition lines. For illustration, we show in Fig. 6 the distribution of torsional angles in the cuboid region for $N=8$, $\rho=0.7$ and $N=9$, $\rho=0.72$ at temperature $T=0.1$. For the $N=8$ polymer, it can clearly be seen that only conformations with torsional angles of 0 and $\pm\pi/2$, i.e., cuboids, occur. For the $N=9$ polymer, these angles are still dominant, although not occurring exclusively. In any case, the existence of that region is in so far worth mentioning as the corresponding conformations do not appear as ground states for this length and as it shows that it is a characteristic feature and not only a length-dependent artifact.

Figure 7 shows the phase diagrams for the longer tubes consisting of $N=10$ and $N=13$ monomers analogously to Fig. 2. In general, beside the short-length artifacts near $T=0$, the phase diagrams at different lengths do not differ qualitatively much from each other. The general thermodynamic behavior is quite similar for all system sizes, especially we find again the four major phases discussed above. Also, the characteristics of the sprawled-coil and bended-ring regions do not depend—beside an obvious shift of the thickness parameter—on the polymer length. We note, however, the onset of the formation of tertiary structures, as also discussed in Ref. [17], especially the helical phase α becomes internally more complex. Furthermore, the relevant thermodynamical activity shifts to lower temperatures.

The ground-state conformations for these systems plotted again in the insets of Figs. 7(c) and 7(d) support our interpretation of the phases given above. Especially the motivation for denoting β the sheet phase becomes clearer, as we found almost planar, "two-dimensional" ground states seeming to crystallize on a honeycomb lattice. These conformations are the dominant conformations in β at finite temperatures as well and form, in the case of the $N=13$ polymer, three LJ contacts, in the sense of a contact map [17]. We find a further interesting detail here, which occurs only for these longer chains. The 13mer is long enough that an intermediate phase β' emerges between β and γ. This phase is populated, as indicated by the ground-state conformation shown in Fig. 7(d), by two small bended circles such that two LJ contacts are formed.
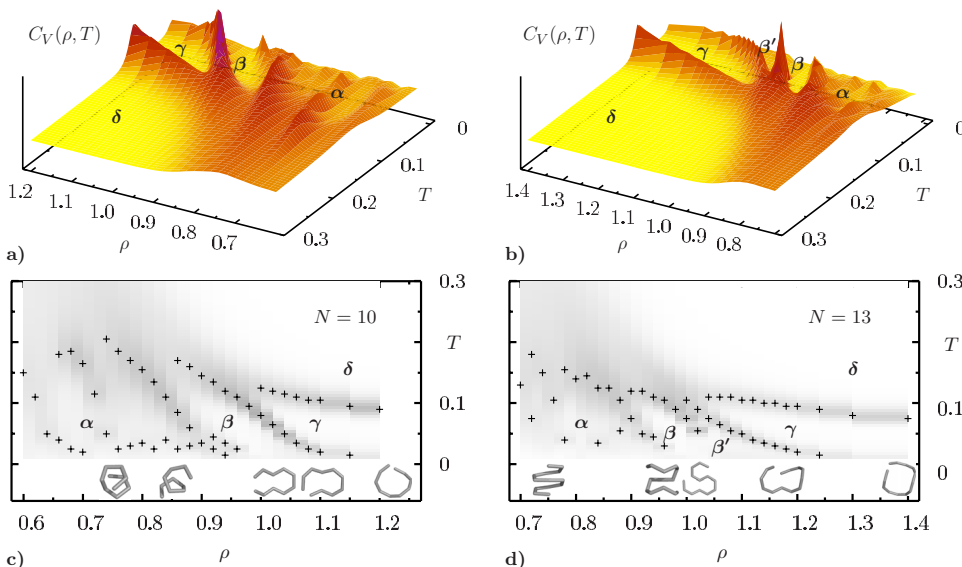

FIG. 7. (Color online) Phase diagrams of the $N=10$ (left) and $N=13$ (right) polymers analogously to Fig. 2.
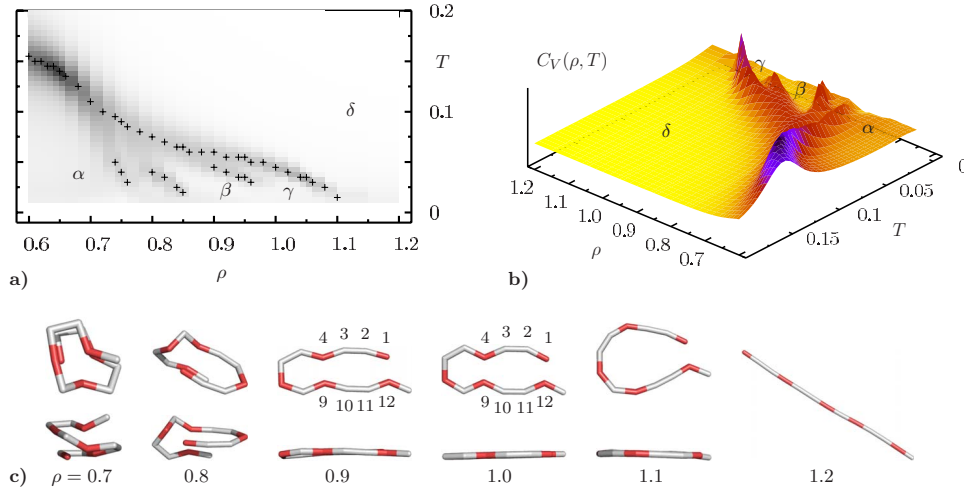
FIG. 8. (Color online) Pseudophase diagram of the $N=13$ Fibonacci AB heteropolymer. (a) The plot shows the top view with marked peak positions of the specific heat for various parameters ρ; (b) the qualitative view of the specific-heat landscape. Grayscales encode the value of the specific heat. The pictures in (c) illustrate selected ground-state conformations. Conformations are shown from different viewpoints: Type-A monomers are marked by red color (dark gray) and B monomers are white.

Since we focus in our study on the very precise investigation of short chains only in order to elaborate the thickness and temperature dependence of secondary-structure formation, noticeable tertiary effects, such as the globular arrangement of secondary-structure segments, are not yet relevant. For longer chains, a classification of structural phases is only possible by accounting for the globular tertiary folding behavior as it was shown in Ref. [14], where proteinlike structures were identified as marginally compact, thus, representing a particular globular conformational phase.

IV. SECONDARY-STRUCTURE PSEUDOPHASES OF A HYDROPHOBIC-POLAR TUBE MODEL

As the central result of this work, we have shown above how the sole introduction of a thickness constraint enhances the formation of different secondary structures, including the helix and sheet formation, for classes of homopolymers. Here, we modify the homopolymer tube model by introducing two species of monomers: hydrophobic (A) and hydrophilic or polar (B) ones. The nonbonded Lennard-Jones interaction between pairs of monomers now depends on their types,

$$V_{\text{LJ}}^{\text{AB}}(r_{i,j}) = 4\left(\frac{1}{r_{i,j}^{12}} - \frac{C(i,j)}{r_{i,j}^6}\right), \qquad (4)$$

where

$$C(i,j) = \begin{cases} +1 & \text{for AA contacts} \\ +1/2 & \text{for BB contacts} \\ -1/2 & \text{for AB contacts.} \end{cases}$$

Besides the strong attraction of A-type monomers, we thus have a weak attraction between B-type monomers and a weak repulsion between monomers of different type, favoring the "hydrophobic" core formation of A monomers. To enable a direct comparison with the literature on the standard

linelike AB model [33,37–39], we introduce here, in addition, a bending term and take the total energy as

$$E_{\text{AB}}(\mathbf{X}) = \frac{1}{4}\sum_k (1 - \cos\vartheta_k) + \sum_{i,j=i+2} V_{\text{LJ}}^{\text{AB}}(r_{i,j}), \qquad (5)$$

where the ϑ_k's are the bending angles of adjacent bond vectors.

Just to acquire a taste for the effects of these changes, we show, as an example, results for the 13mer Fibonacci sequence $\text{AB}_2\text{AB}_2\text{ABAB}_2\text{AB}$, which has been studied in the linelike AB model, i.e., with $\rho=0$, some time ago [33,38,39]. Figure 8 shows the phase diagram analogously to Figs. 2 and 7, as well as selected ground-state conformations. The general structure including several separated structural subphases is similar to that for the presented homopolymers. The most prominent finding is definitely the very stable β-sheet region in the interval $0.90 \leq \rho \leq 1.01$, as $T \to 0$. The conformations there are neither of κ_0 nor τ_0 type, i.e., they have neither constant bond nor torsion angles [17]; but they are indeed "planar" (data not shown, see Fig. 8 for visualization). These qualitative properties do not change over the entire region. A quantitatively remarkable fact is the variation in the intramonomer distances. We note that the interaction length between the opposite hydrophobic A monomers 1–12 [$r_{1,12}=1.13$, see Fig. 8(c) for monomer numbering] and 4–9 ($r_{4,9}=1.15$) in the sheet conformation does not change in the whole thickness region at all. On the other hand, the distances between the B monomers 2–11 and 3–10 increase ($\Delta r_{2,9} = \Delta r_{3,10} = 0.27$) and decrease between the A monomers 1–4 and 9–12 ($\Delta r_{1,4} = \Delta r_{9,12} = -0.10$, differences respecting the conformations at $\rho=0.9$ and $\rho=1.0$). The van der Waals attraction between the A monomers is thus the dominant factor that stabilizes the β sheet. Remarkably, as becomes clear by the listed geometrical quantities above, the bending energy is even increasing with increasing thickness in this region—contrarily to the general overall trend that the bend-

ing energy decreases with increasing thickness. We discuss the influence of the bending term further below. Remember that there are planar six-ring conformations at comparable thicknesses for the $N=8$, $N=10$, and $N=13$ homopolymer ground states [17]. These structures are now stabilized by the specific monomer sequence. We emphasize that the tube thickness keeps playing an important role. Just simulating the given sequence in a two-dimensional space without thickness leads to completely different conformations, consisting of a hydrophobic core and a polar shell [38].

At lower thickness parameters, we find structures with helical properties, which, however, depend on the monomer sequence. We note here a very pronounced conformational transition from random coils to native conformations at 0.1 $\lesssim T \lesssim 0.15$, which is in detail discussed for the linelike limit "$\rho \lesssim 0.6$" in Ref. [33]. With increasing thickness, the ground-state conformation becomes a ring and finally switches to a stretched rod, which—contrarily to the homopolymers discussed above—appears as a ground-state conformation. This is a qualitative difference to the results in Sec. III.

Finally, two remarks are in order. First, using the described model, we make two independent changes compared to the homopolymer model used before. We introduce different kinds of monomers with different interactions and in addition a bending stiffness. To evaluate the influence of each of the two changes, we simulated the 13mer with a homopolymer sequence consisting of just hydrophobic A monomers (A_{13}), which is equal to the homopolymer studied without bending stiffness in Sec. III. We made sure that the influence of the bending stiffness is marginal for both ground-state structures and thermodynamical behavior in the relevant structural regions. The ground-state energies change by 1–5 % in the α and β regions, the structures themselves remain qualitatively the same. The effect on the thermodynamical behavior is marginal, in particular, peak positions in the specific heat are not influenced. We conclude, therefore, that the described behavior is predominantly based on the influence of different monomer types. Remember also the example discussed above on this observation. Note that choosing a B homopolymer (B_{13}) would correspond to $\sigma = 2^{1/6}$ and $\epsilon = 1/4$ in Eq. (1), with $r_{i,j}^{\mathrm{opt}} = 2^{1/3}$ and $V_{\mathrm{LJ}}(r_{i,j}^{\mathrm{opt}}) = -1/4$. Absorbing the energy scale in the definition of temperature (i.e., $\epsilon = 1/4 \rightarrow \epsilon_B = 1$), we would work with $T_B = T_A/4$.

Second, as a methodological remark, knowing that ground states of one-dimensional linelike models do intrinsically have some measurable "natural thickness" $d(\mathbf{X})$ in the interpretation of the global radius of curvature [see Eq. (2)], it may be favorable to search for ground states by simulating the polymer with a thickness constraint slightly below this value. One restricts the conformational space significantly and may travel much faster through the remaining phase space. That way, we could confirm for the 13mer Fibonacci sequence and other widely used AB polymers with $N \leq 21$ monomers the ground-state energies and conformations presented over the past years [33,40–42].

V. SUMMARY

We present in this paper the results of a computer simulation study of the thermodynamical behavior of a tube model for simple homopolymers as well as for an exemplified hydrophobic-polar heteropolymer. The thickness of the tube in our simulations is controlled by a single parameter, the global radius of curvature, which depends on three-body interactions [43].

After focusing on ground states of homopolymers and their properties in a previous work [17], we identified dominant structural pseudophases at finite temperatures, i.e., specific-heat landscapes depending on the thickness parameter and temperature, representing the conformational phase diagram. Independently of the polymer length, we find four major structural phases. These include helices, sheetlike planar structures, bended rings, and sprawled random coils. These different secondary-structure phases can be assigned to different ranges of the tube thickness. The thickness parameter is therefore suitable for a classification of the secondary structures of polymers. Concentrating on the analysis of the secondary-structure formation of short chains, tertiary effects could widely be excluded. Symmetries and anisotropy in the arrangement of secondary-structure segments in globular domains [14], which are particularly interesting for proteins, are necessarily of importance in the discussion of the folding behavior of longer chains. A precise investigation of the thickness-dependent influence of thermal fluctuations on the phase structure is future work.

In an extension of the tube polymer concept, we also introduced the AB tube model for hydrophobic-polar heteropolymers and discussed results for a given sequence of monomers, which has extensively been studied before without thickness. We showed that a sequence of hydrophobic and polar monomers can stabilize the general secondary structures. In particular, we find a very pronounced and stable region of a β-sheet structure.

Our results are qualitative in a sense that they represent the general frame of possible conformational phases of secondary structures for thick polymers and proteins. This is the basis for further analyses of pseudophases of models designed for specific polymers or proteins.

To conclude, the tube picture is well suited to mimic the volume extension of polymers, for example, due to side chains of amino acids in biopolymers. It may be employed in other contexts as well, for example, for simulations of a tube model for entangled networks of polymers, where the hypothetical tube around a polymer models the suppression of the transverse undulation by the network [3,44]. Finally, also the diffusion of knots in knotted DNA can proceed via the solitonic diffusion of compact knot shapes [45]. The tube picture also may be applicable here.

[1] *Monte Carlo and Molecular Dynamics Simulations in Polymer Science*, edited by K. Binder (Oxford University Press, New York, 1995).

[2] P. J. Flory, *Principles of Polymer Chemistry* (Cornell University Press, Ithaca, 1953).

[3] P.-G. de Gennes, *Scaling Concepts in Polymer Physics* (Cornell University Press, Ithaca, 1979).

[4] P. Grassberger, Phys. Rev. E **56**, 3682 (1997).

[5] T. Vogel, M. Bachmann, and W. Janke, Phys. Rev. E **76**, 061803 (2007).

[6] S. Schnabel, T. Vogel, M. Bachmann, and W. Janke, Chem. Phys. Lett. **476**, 201 (2009).

[7] H. Noguchi and K. Yoshikawa, J. Chem. Phys. **109**, 5070 (1998).

[8] J. P. Kemp and Z. Y. Chen, Phys. Rev. Lett. **81**, 3880 (1998).

[9] D. C. Rapaport, Phys. Rev. E **66**, 011906 (2002).

[10] S. A. Sabeur, F. Hamdache, and F. Schmid, Phys. Rev. E **77**, 020802(R) (2008).

[11] J. R. Banavar, A. Flammini, D. Marenduzzo, A. Maritan, and A. Trovato, J. Phys.: Condens. Matter **15**, S1787 (2003).

[12] J. R. Banavar, O. Gonzalez, J. H. Maddocks, and A. Maritan, J. Stat. Phys. **110**, 35 (2003).

[13] J. R. Banavar, T. X. Hoang, A. Maritan, F. Seno, and A. Trovato, Phys. Rev. E **70**, 041905 (2004), and references therein.

[14] T. X. Hoang, A. Trovato, F. Seno, J. R. Banavar, and A. Maritan, J. Phys.: Condens. Matter **18**, S297 (2006).

[15] J. R. Banavar and A. Maritan, Annu. Rev. Biophys. Biomol. Struct. **36**, 261 (2007).

[16] T. Vogel, T. Neuhaus, M. Bachmann, and W. Janke, EPL **85**, 10003 (2009).

[17] T. Vogel, T. Neuhaus, M. Bachmann, and W. Janke, Eur. Phys. J. E (to be published).

[18] M. Bachmann and W. Janke, J. Chem. Phys. **120**, 6779 (2004).

[19] T. X. Hoang, A. Trovato, F. Seno, J. R. Banavar, and A. Maritan, Proc. Natl. Acad. Sci. U.S.A. **101**, 7960 (2004).

[20] Y. Snir and R. D. Kamien, Science **307**, 1067 (2005).

[21] Y. Snir and R. D. Kamien, Phys. Rev. E **75**, 051114 (2007).

[22] S. Auer, M. A. Miller, S. V. Krivov, C. M. Dobson, M. Karplus, and M. Vendruscolo, Phys. Rev. Lett. **99**, 178104 (2007).

[23] K. Wolff, M. Vendruscolo, and M. Porto, Gene **422**, 47 (2008).

[24] O. Gonzalez and J. H. Maddocks, Proc. Natl. Acad. Sci. U.S.A. **96**, 4769 (1999).

[25] T. Neuhaus, O. Zimmermann, and U. H. E. Hansmann, Phys. Rev. E **75**, 051803 (2007).

[26] B. A. Berg and T. Neuhaus, Phys. Lett. B **267**, 249 (1991).

[27] B. A. Berg and T. Neuhaus, Phys. Rev. Lett. **68**, 9 (1992).

[28] F. Wang and D. P. Landau, Phys. Rev. Lett. **86**, 2050 (2001).

[29] C. Zhou and R. N. Bhatt, Phys. Rev. E **72**, 025701(R) (2005).

[30] K. Hukushima and K. Nemoto, J. Phys. Soc. Jpn. **65**, 1604 (1996).

[31] C. Geyer, in *Computing Science and Statistics, Proceedings of the 23rd Symposium on the Interface*, edited by E. Keramidas (Interface Foundation, Fairfax Station, VA, 1991), p. 156.

[32] E. Bittner, A. Nußbaumer, and W. Janke, Phys. Rev. Lett. **101**, 130603 (2008).

[33] M. Bachmann, H. Arkin, and W. Janke, Phys. Rev. E **71**, 031906 (2005).

[34] J. B. Tenenbaum, V. de Silva, and J. C. Langford, Science **290**, 2319 (2000).

[35] H. S. Chan and K. A. Dill, J. Chem. Phys. **92**, 3118 (1990).

[36] The occurrence of these structures as ground states for certain system sizes, e.g., the crystallization on regular lattices as singular solutions of the theory, has been analyzed and discussed in detail in Ref. [17].

[37] F. H. Stillinger, T. Head-Gordon, and C. L. Hirshfeld, Phys. Rev. E **48**, 1469 (1993).

[38] F. H. Stillinger and T. Head-Gordon, Phys. Rev. E **52**, 2872 (1995).

[39] H.-P. Hsu, V. Mehra, and P. Grassberger, Phys. Rev. E **68**, 037703 (2003).

[40] S.-Y. Kim, S. B. Lee, and J. Lee, Phys. Rev. E **72**, 011916 (2005).

[41] V. Elser and I. Rankenburg, Phys. Rev. E **73**, 026702 (2006).

[42] W. Huang, M. Chen, and Z. Lü, Phys. Rev. E **74**, 041907 (2006).

[43] For the advantages of this implementation and differences to realizations with pairwise repulsive potentials, we refer the reader to the discussions in Refs. [12,16].

[44] H. Hinsch, J. Wilhelm, and E. Frey, Eur. Phys. J. E **24**, 35 (2007).

[45] A. Y. Grosberg and Y. Rabin, Phys. Rev. Lett. **99**, 217801 (2007).